A PALEOCEANOGRAPHIC RECONSTRUCTION OF NORTH ATLANTIC OCEAN CIRCULATION

by

Erin Leathrum

A thesis submitted to the Faculty of the University of Delaware in partial fulfillment of the requirements for the degree of Honors Degree in Major with Distinction

Spring 2022

A PALEOCEANOGRAPHIC RECONSTRUCTION

OF NORTH ATLANTIC

OCEAN CIRCULATION

by

Erin Leathrum

Approved: _____

Thesis Director's Name, Highest Degree
Professor in charge of thesis on behalf of the Advisory Committee

Approved: _____

Second Reader's Name, Highest Degree
Committee member from the Department of Department Name

Approved: _____

Third Reader's Name, Highest Degree
Committee member from the Board of Senior Thesis Readers

Approved: _____

Michael Chajes, Ph.D Dean of Honors College

ACKNOWLEDGMENTS

TABLE OF CONTENTS

LIST OF TABLES

LIST OF FIGURES

ABSTRACT

This project applies *Globorotalia truncatulinoides* coiling ratios as a proxy for changes in upper ocean hydrography and gyre circulation in the northeastern region of the North Atlantic subtropical gyre over the past 140 thousand years, covering both glacial and interglacial intervals. We used sediment cores from Integrated Ocean Drilling Program Site U1313 to assess the changes in coiling variety. In the modern ocean, this gyre region displays a deep permanent thermocline, favoring the left coiling (sinistral) form. At Site U1313 there are variations in percent sinistral during the warm interglacial interval Marine Isotope Stage 5 (MIS 5) with an increase in the dextral form during the colder substages MIS 5a and c. Previously published sites underneath the western boundary current (Site KNR140-37 PC) and in the center of the gyre (Integrated Ocean Drilling Program Site 1063) show that the percent sinistral stays high throughout interglacial intervals, including MIS 5, and the right coiling (dextral) form dominates during glacial periods. This study's results are different than previously published data, as there are exceptions to the glacial versus interglacial trend during MIS 5, which suggests a change in gyre circulation and intensity not previously reconstructed. Further comparison to the previously published sites and analysis of additional subpolar sites will help interpret the hydrographic changes occurring in the North Atlantic subtropical gyre.

Chapter 1

INTRODUCTION

The coiling direction of planktic foraminifera *Globoratalia truncatulinoides* has previously been studied as a proxy for the upper ocean dynamics at sites near the North Atlantic subtropical gyre over different time intervals (Feldmeijer et al., 2014; Billups et al., 2016; Kaiser et al., 2019; Billups et al., 2020, Figure 1). In particular, the coiling direction reflects the depth of the permanent thermocline because this is the depth near which G. *truncatulinoides* calcify their shells (Figure 2). In the upper ocean, the depth at which the surface mixed layer separates from the deeper water and experiences a rapid temperature change is called the permanent thermocline (Talley, 2011). The relative depth of the permanent thermocline varies over glacial to interglacial cycles and illustrates changes in the upper ocean hydrographic parameters of the subtropical gyre circulation (Feldmeijer et al., 2014). Hydrographic parameters such as changes in gyre placement and the strength of the Gulf Stream affect the warm water advection across the North Atlantic Gyre and affect the depth of the permanent thermocline.

In the North Atlantic, *G. truncatulinoides* exhibit two coiling directions, left and right, each favoring different environmental conditions. In brief, the left coiling (sinistral) form inhabits areas of the gyre characterized by a deep permanent thermocline (Feldmeijer et al., 2014). The right coiling (dextral) form inhabits areas with a shallow thermocline. Therefore, the difference in coiling directions downcore

can provide information about surface waters and ocean circulation over geological time.

The circulation of the gyre moderates the climate system in the North Atlantic due to the transport of heat towards higher latitudes, affecting the temperature of the surface waters and thermocline (Schmitz, 1996). The North Atlantic subtropical gyre has an important influence on the global transport of heat. The western boundary current of the North Atlantic subtropical gyre, the Gulf Stream, and its extension, the North Atlantic Current, transport heat northward and moderate Europe's climate. The heat transport across North America's east coast from the Gulf stream also helps regulate regional temperatures in North America (Stommel, 1948). The poleward transport of heat is vital to the formation of deep water in the North Atlantic, which contributes to global overturning circulation (Schmitz, 1996). Changes in the circulation of the gyre can influence the ocean-atmospheric interaction and results in changes to the regional climate (Marshall et al., 2001). For example, the interannual climate variation, the North Atlantic Oscillation is a periodic ocean-atmospheric oscillation with changes in the strengths of the atmospheric low-pressure region near Iceland and the subtropical high-pressure zone near the Azores (Marshall et al., 2001). When the pressure gradient between the two zones weakens, there Europe experiences harsher winters. The North Atlantic Oscillation is responsible for most of the climate variability in the North Atlantic and the intensity of the North Atlantic overturning circulation. The North Atlantic Oscillation varies over geologic time as it has been directly linked to changes in the sea ice in the North Atlantic (Marshall et al., 2001).

The climate variations and circulation of the gyre vary over time during glacial and interglacial cycles (Marshall et al., 2001; Rahmstorf et al., 2002). Analyzing the

changes in *G. truncatulinoides* coiling ratios downcore over several glacial and interglacial intervals provides information about the role of the gyre in the climate system as it represents characteristics of the upper water column above the sites. Previous studies using G. *truncatulinoides* coiling ratios as a proxy for the western boundary current and North Atlantic gyre hydrography showed differences in gyre intensity and placement over glacial to interglacial intervals (Billups et al., 2016; Kaiser et al., 2019; Billups et al., 2020). For example, during several glacial intervals, the northern gyre boundary was reconstructed as a shift southward toward the equator with a weakened flow of the Gulf Stream. The change during glacial intervals was illustrated by a lack of percent sinistral at lower latitude sites, indicating weakened circulation and southward displacement. The increased percent sinistral during interglacial intervals led to a reconstruction of gyre flow showing intensification of the western boundary current and placement similar to the modern interglacial.

This study uses Integrated Ocean Drilling Program (IODP) Site U1313, located underneath the northern boundary current, the Azores Current (Figure 1), to contribute new information about the hydrography of the gyre boundary. The drill site sits on the northwestern sideof the Mid-Atlantic Ridge. Site U1313 reoccupies the Deep-Sea Drilling Project Site 607 (W.F. Ruddiman, A. McIntyre, and M. Raymo, 1987), which was previously studied for the use of *G. truncatulinoides* as a palaeoceanographic proxy during the Pleistocene from 1200 - 400 ka (Kaiser et al., 2019). Modern oceanographic glider data indicate that the North Atlantic Current influences the surface waters at Site U1313 because of its recirculation off the Grand Banks (Voelker et al., 2010). Due to the warm water influence from the North Atlantic Current, this region experiences a deep permanent thermocline (~300 m) and a strong seasonal

thermocline (Channel et al., 2006; Voelker et al., 2010; Kaiser et al., 2019), (Figure 2). Therefore, the surface layer core data from this region shows that present environmental conditions favor the left coiling variety (sinistral form) (Kaiser et al., 2019; Kucera et al., 2005). I hypothesize that relative differences in the coiling ratios over time would illustrate changes in warm water advection coming from the Gulf Stream and its continuation of the North Atlantic Current and/or the Azores Current over glacial and interglacial intervals. The time interval in this study covers 140 ka (thousand years) ago to the present, representing two major interglacial intervals and two glacial intervals. Covering both a glacial and interglacial interval can provide an overview of the changes in the circulation of the gyre around Site U1313 during climate cycles.

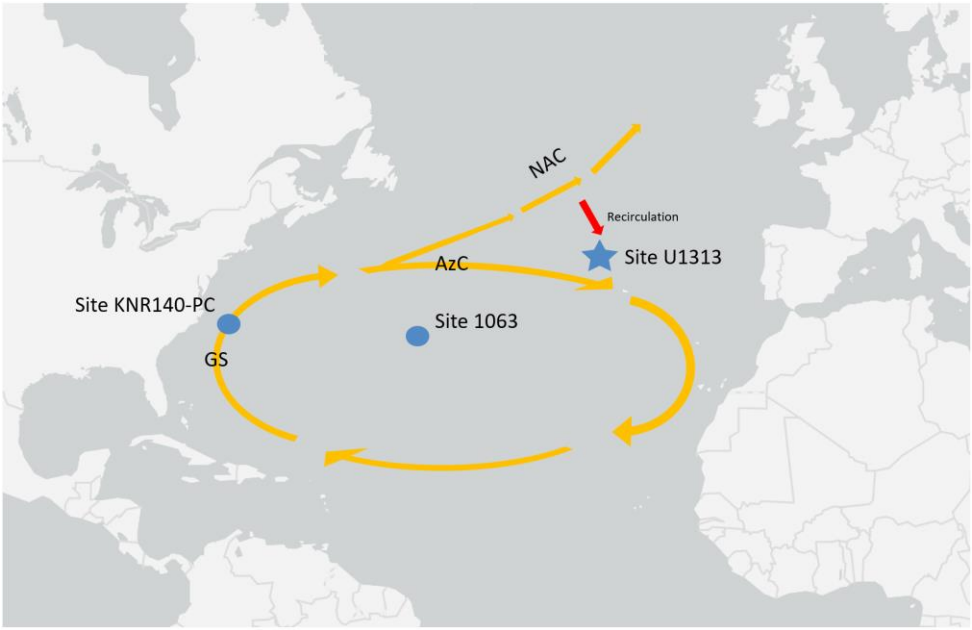

Figure 1: Map of North Atlantic subtropical gyre with labeled currents. Abbreviations are as follows: Gulf Stream (GS), Azores Current (AzC), and North Atlantic Current (NAC). Star indicates the approximate placement of Site U1313. Circles indicate sites for which (Ocean Drilling Program ODP 1063 and Piston core KNR140-37PC) Globorotalia truncatulinoides coiling direction data were previously published (Billups et al. 2016; Billups et al. 2020). Image created from Arc GIS Pro.

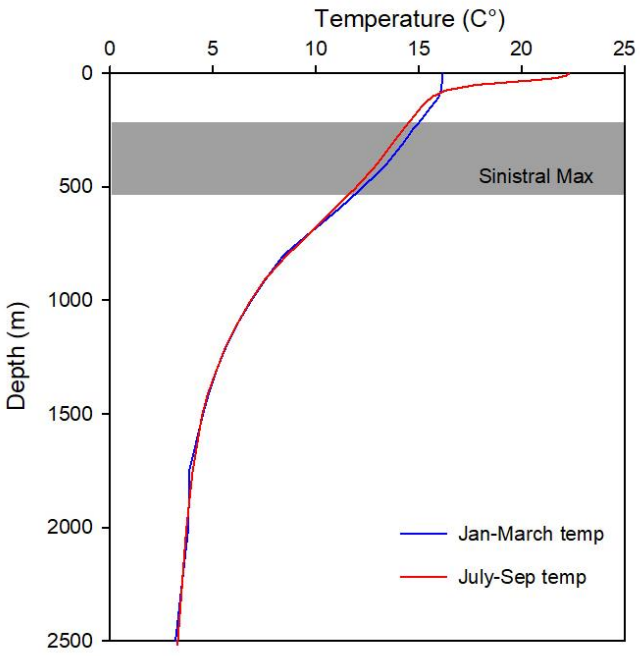

Figure 2: Water column temperature profile from Site U1313 with the two seasonal extremes (January to March in blue & July to September in red). The permanent thermocline is located 500m below the sea surface. The grey box indicated the depth at which the sinistral form dominates (~300m) (Ujiie et al., 2010; Feldmeijer et al., 2014). The figure was created from data from LDEO interactive website.

Chapter 2.

BACKGROUND

2.1 Glacial to Interglacial Cycles and Oxygen Isotopes

The force that drives Earth's climate system over time is the cyclic changes in Earth's orbital geometry, as first defined by Milankovitch (1941). These changes are all driven by differences in Earth's eccentricity, obliquity, and precession (Berger, 1978) and affect insolation, defined as the amount of solar radiation that hits the earth at one time. Eccentricity affects the distance and shape of the Earth's orbit around the Sun. Earth's obliquity describes the changes in the tilt of Earth's axis and accounts for large insolation changes because a large tilt angle increases seasonal differences at high latitudes. Precession refers to the wobble of the Earth around its axis, and it alters the position of Earth's solstices and equinoxes on the Earth's orbit around the sun. These orbital parameters together change the distance between the Sun and Earth and the occurrence of seasons in Earth's orbit. As originally proposed by Milankovitch, the changes in seasonal summer insolation are the primary factor driving Earth's climate at high latitudes and glacial-interglacial cycles. Ice growth occurs when summer insolation reduces, and ice sheets melt when the amount of summer insolation increases again. The variations in orbital parameters have precise ages, as calculated by Milankovitch (1941) and Berger (1978). Variations in ice sheet size affect the geochemistry of seawater and are recorded in marine carbonates (Shackleton, 1968). Therefore, it is possible to use marine carbonates to reconstruct glacial to interglacial cycles. It is also possible to date marine carbonates by comparing the variations in geochemical trends, such as isotope ratios, to the

calculated ages of an insolation curve. This is a commonly used stratigraphic technique for dating the glacial and interglacial cycles

Oxygen isotope ratios in seawater are linked to glacial/interglacial cycles because of water's oxygen isotope fractionation in the hydrological cycle (Faure, 1991; Libes, 2009; Ruddiman, 2014). Emiliani (1955) first introduced the concept of isotope stratigraphy. As oxygen is present on the water molecule (liquid and vapor phase), major water reservoirs such as the ocean and ice sheets exchange isotopically depleted or enriched water molecules over geologic time. The weight of the isotopes contributes to how the water molecules interact in the hydrologic cycle. The H_2O molecule with the lighter isotope evaporates more easily ($H_2{}^{16}O$) and is extracted from the ocean at low latitudes and transported to higher latitudes. In contrast, as water condenses, more $H_2{}^{18}O$ molecules are lost and rained out as the traveling air mass moves poleward. Therefore, water vapor that reaches the higher latitudes and contributes snow to ice sheets is enriched in ^{16}O. Due to the lack of melting of the ^{16}O enriched ice sheets in glacial intervals, the ocean waters are enriched in ^{18}O. As foraminifera calcify their carbonate shells in the water column, they reflect the isotopic composition of the water in which they grow. The planktic or benthic foraminifera eventually die and create the sediment layers on the ocean floor. The ratio of oxygen isotopes in the foraminifera shells shows glacial intervals have higher $^{18}O/\ ^{16}O$ ratios and interglacial intervals have lower ratios (Emiliani, 1955). The ratios of $^{18}O/\ ^{16}O$ in water and carbonates are small, so they are calculated as deviations ("delta-values") from a global standard in parts per thousand (Faure, 1991).

The benthic foraminifera age stack published by Lisiecki and Raymo (2005) (LR04) is a widely used palaeoceanographic standard for deriving age models in this

manner because benthic foraminifera reflect the $\delta^{18}O$ of deep water. The deep-water $\delta^{18}O$ data reflects overall changes in ice volume and is not as sensitive to local variations of temperature (Faure, 1991). The age stack compiles benthic $\delta^{18}O$ data from 57 globally distributed sites spanning 5.3 million years. (Lisiecki and Raymo, 2005). Ages for this stack were derived by adjusting glacial/interglacial cycles as recorded by $\delta^{18}O$ values to northern hemisphere summer insolation (Figure 3). Benthic foraminiferal variations of $\delta^{18}O$, such as the LR04 age stack, provide context to all palaeoceanographic studies and can be separated into glacial versus interglacial Marine Isotope Stages (MIS) initially defined by Emiliani et al. (1955) and Shackleton (1968). In my study, the lettering of these MIS and their substages (e.g., MIS 5a-e) follow Railsback et al. (2015). This study covers 140 thousand years, spanning interglacial intervals MIS 1, 3, and 5 and glacial intervals MIS 2, 4, and 6.

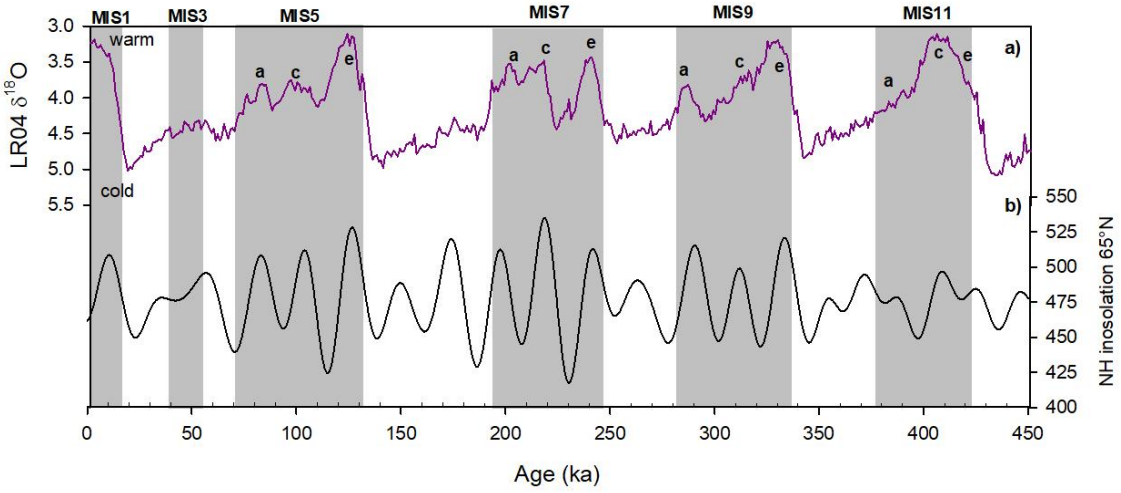

Figure 3: Figure showings comparison between insolation and $\delta^{18}O$ that Lisiecki and Raymo (2005) used for their age stack tuning process. Panels are as follows: a) the $\delta^{18}O$ LR04 age stack b) June insolation at 65°N in the Northern Hemisphere (NH). Each $\delta^{18}O$ minimum corresponds with an insolation maximum.

2.2 Proxy: *Globorotalia truncatulinoides*

The planktic foraminiferal species *G. truncatulinoides* has five different morphotypes (I-V), exhibiting calcareous shells that form a coiling spiral. These morphotypes inhabit different locations across the globe. Type I, II, and V live in warm waters and are physically larger than subpolar types III and IV. Type I inhabits warm subtropical water in the Southern Hemisphere. Type III and IV are found primarily in the cold subpolar frontal zones of the Southern Ocean, and type V inhabits the northwest Pacific (de Vargas et al., 2001; Quillevere et al., 2011). Morphological differences appear in each type, but all exhibit a large conical shape that coils either to the left or right. The morphotype that inhabits the North Atlantic and was previously explored for proxy use, Type II, exhibits two different coiling directions, sinistral (left coiling) and dextral (right coiling) (Ujiie et al., 2010; Feldmeijer et al., 2014) (Figure 4). The two different coiling directions calcify under different environmental conditions; therefore, the coiling direction of *G. truncatulinoides* reflects the water masses determining the depth of the permanent thermocline (Feldmeijer et al., 2014).

The coiling direction ratios of G. *truncatulinoides* Type II were used directly as a proxy for changes in the relative depth of the permanent thermocline in Feldmejier et al. (2014) and Kaiser et al. (2019), but they were first used as an environmental tracer by Ericson et al. (1955). Planktonic tows and surface core measurements show that the dextral form prefers colder, nutrient-rich waters in gyre margins (Kucera et al., 2005). In contrast, the sinistral form calcifies at deep, permanent thermoclines with seasonal deep mixing and phytoplankton blooms present in the winter (de Vargas et al., 2001; Feldmeijer et al., 2014). Modern ocean conditions that experience a deep thermocline include gyre boundaries and the center

of the gyre. (Ericson et al., 1955; Renaud and Schmidt, 2003; Ujiie et al., 2010; Feldmeijer et al., 2014).

Changes in the dominant coiling direction downcore indicate the upper-ocean hydrography over time, but more specifically, the depth of the permanent thermocline. Kaiser et al. (2019) interpret the increase in percent sinistral at the subtropical and subpolar sites as an increase in poleward warm water advection, resulting in a deeper thermocline in those regions. In their study, the abundance of the coiling ratios downcore over time from multiple core sites gave an overall view of the depth of the thermocline during the climate cycles in the mid-Pleistocene Transition (~1200- 400 ka). Therefore, the dominant coiling direction reflects upper ocean hydrography, and I should be able to use it to reconstruct the depth of the thermocline for the northern boundary Site U1313 from the past 140 ka. Additionally, I can infer parameters, such as warm water advection, influencing the depth of the thermocline over glacial and interglacial intervals.

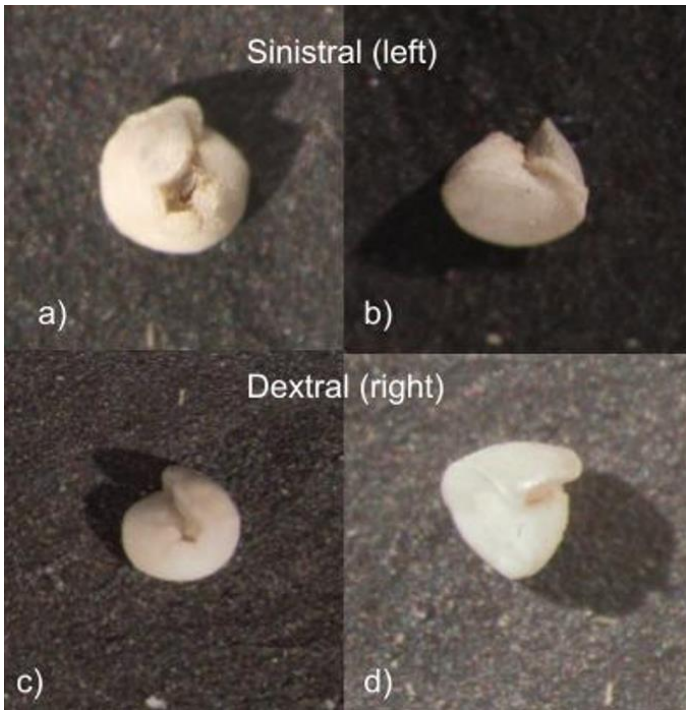

Figure 4: Left coiling (sinistral) form of *Globoratalia truncatulinoides.* The top view is dorsal side up (Ericson et al., 1955). Panels are as follows: a) dorsal side up sinistral form; b) dorsal side down sinistral form; c) dorsal side up dextral form; d) dorsal side down dextral form

Chapter 3

METHODS

3.1 Sampling

The samples used in this study come from sediment cores taken at IODP Site U1313 from the JOIDES Resolution research vessel (Channel et al., 2006). The depth of the sampled core intervals corresponds to the ages from 1.75 ka to 140 ka (thousand years ago), spanning the late Pleistocene period to the Holocene. The sediment samples from Site U1313 are 2-3 cm slices, or plugs, sampled every 5 cm from the surface layer to 6.88 meters below the seafloor. The sampling strategy provides temporal overlap with percent sinistral data from previously published studies using G *truncatulinoides* as a proxy (KNR140-37PC and IODP Site 1063, Billups et al., 2016; Billups et al., 2020).

3.2 Age Model

The age model of Site U1313 is based on comparing downcore variation in the color of the sediment, or L parameter, to the variations in foraminiferal oxygen isotopes in the LR04 stack (Figure 5, Channel et al., 2006). The L parameter of Site U1313, and the benthic foraminiferal $\delta^{18}O$ stack by Lisiecki and Raymo (2005), show similar variations illustrating the glacial/interglacial patterns (Channel et al., 2006). The L parameter, or color stratigraphy, measures the lightness of the sediment particles in the core. Dark clay sediments represent glacial intervals with low carbonate and high $\delta^{18}O$ values, while the lighter sediments represent the interglacial intervals with high carbonate and lower $\delta^{18}O$ values. Given the derived age-depth control points published by Channel et al. (2006), I used the Arrand software package

from Howell et al. (2006) to interpolate the ages for the 5 cm sampling intervals used in this study, which cover 1.75 to 140 ka.

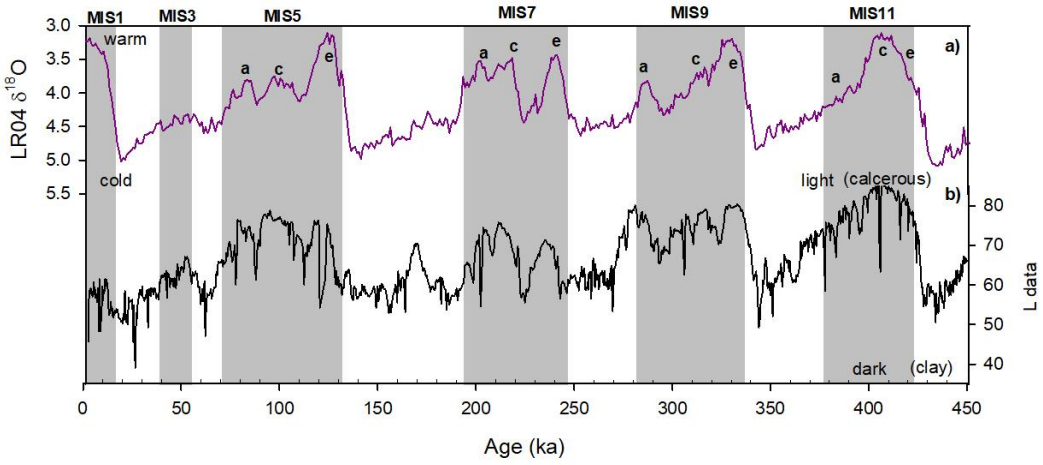

Figure 5: Shows the LR04 benthic age stack and the L parameter data at Site U1313 from 0 to 450 ka. Panels are as follows: a) LR04 age stack (Lesieki and Raymo, 2005); b) L parameter data at site U1313 (Channel et al., 2006). The grey boxes are the warm interglacial periods, and the white boxes are the cold glacial periods. The lettering of Marine Isotope Stages comes from Railsback et al. (2014), with odd-numbered stages as interglacial intervals.

3.3 Laboratory Work

The sediment samples were processed using standard procedures to have the clean and correct size fraction for foraminiferal content underneath a microscope. The sediments were processed by drying overnight in an oven, recording the dry weight, and then soaking in a buffered sodium metaphosphate solution (20 g sodium metaphosphate, 10 L deionized water, 2 ml ammonium hydroxide) and wet sieved at >63µm. The dried samples are transferred and stored in labeled vials.

In order to pick foraminifera, most of the samples were further size fractionated to isolate the 335 - 500 μm size fraction (adult samples according to Feldmeijer et al., 2014). This size fraction leaves large test count abundances (>20 counts) on the sample tray for counting. Counts of >20 do not introduce bias at other sites using the same proxy (Billups et al. 2016, Billups et al. 2020, & Kaiser et al. 2019). If the samples at the 335 - 500 μm size fraction yielded large counts, they were split 1-3 times for counting. Only one split was counted, and then the total in the sample was calculated based on the number of splits. During glacial extremes, a few samples yielded counts <20. To increase the count size to fully understand if there were significant percent sinistral changes, the intervals with <20 were counted at both the 335 - 500 μm and the 250-335 μm size fraction. Percent sinistral was calculated by dividing the number of sinistral by the total abundance from combined splits of dextral and sinistral counts and multiplying by 100 (#sinistral/ #sinistral + #dextral * 100). Percent sinistral changes are considered "dominating" the population if their percentage lies above 50%.

Previous work showed only a small difference between percent sinistral across size fractions (Ujiie et al., 2010; Feldmeijer et al., 2014; Kaiser et al., 2019). Feldmeijer et al. (2014) tested the size fractions 212-250 μm, 250-300 μm, 300-355 μm, and 355-400 μm separately and were able to show that percent sinistral was comparable at each. To test if Site U1313 followed the same pattern as the previously published studies, I tested the 250-355 μm size fraction on intervals from U1313C Hole 1 Section 1 32 cm to 54 cm for counts >20. The sinistral counts were comparable as the average difference is low (~5%, dark gray in Table 1). Since the difference in the >20 counts were small, I do not believe combining size fractions introduces any

noise or bias. The average difference in the counts <20 is large (~14.5%, light gray in Table 1). The percent sinistral below 20 counts become too variable, so I exclude counts that are <20 after the combined size fraction from the final data. Counts <20 from both combined size fractions only occur during part of interglacial MIS 2, with 12 intervals with <20 counts. I can exclude the counts <20 during the glacial interval MIS 2 because a high percentage (93.3%) of the samples from Site U1313 are above 20 counts after combining fractions when needed. (Figure 6). All data collected here are summarized in Appendix 1.

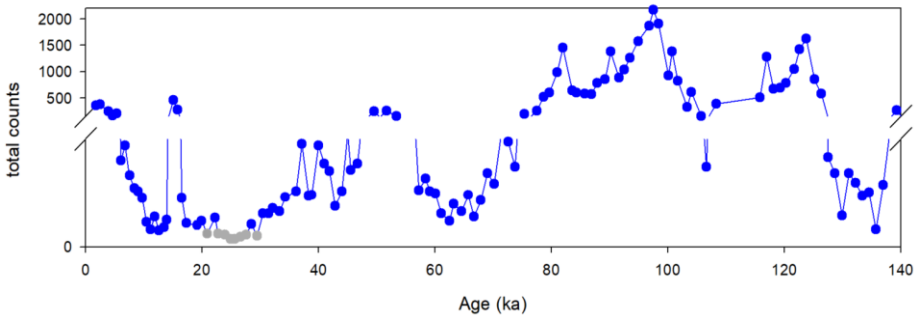

Figure 6: Total abundance of sinistral and dextral tests from Site U1313. Light grey dots indicate intervals where test counts were <20 even with the combined size fractions.

Count size	Interval	%sin >250	%sin >350	Difference %	Ave. diff.	St. dev
	U1313 C H1-1 32-34 cm	58.1	49.1	9		
	U1313 C H1-1 37-39 cm	47.9	55.2	7.3		
>20	U1313 C H1-1 42-44 cm	47.5	46.3	1.2	5.52	2.95
	U1313 C H1-1 47-49 cm	38.1	43.6	5.5		
	U1313 C H1-1 52-54 cm	30.4	25.8	4.6		
	U1313 C H1-1 72-74 cm	44.4	42.9	1.5		
	U1313 C H1-1 77-79 cm	40	36.4	3.6		
<20	U1313 C H1-1 87-89 cm	50	22.2	27.8	14.5	12.80
	U1313 C H1-1 93-95 cm	57.1	45.5	11.6		
	U1313 C H1-1 96-98 cm	33.3	5.3	28		

Table 1: Shows percent sinistral in each size fraction and differences from a select amount of interval with counts>20 (dark grey) and counts <20 (light gray). The average difference and standard deviation are calculated from both intervals >20 and <20.

Chapter 4

RESULTS

4.1 Total Abundance of *Globorotalia truncatulinoides*

The total abundance was calculated from the total counts of both sinistral and dextral forms of *G. truncatulinoides* from each sample, as described in section 3.3. Overall, the total abundance trend follows closely with the glacial and interglacial pattern when compared to the LR04 age stack (Figure 7a). The total abundance varies throughout our study interval from minima <20 (plotted as gaps in the record) to a maximum of 2175 counts (Figure 7b). The total abundance stays high during interglacial periods such as the late Holocene and shows a maximum during interglacial MIS 5. The total abundance shows another maximum during the moderate interglacial MIS 3 (~ 50 ka). The total abundance stays low and reaches its minimum of <20 during the glacial periods of MIS 2. During the last deglaciation (~14 ka) the total abundance reaches a maximum and decreases slightly during MIS1 but remains relatively high.

Although, the total abundance data shows finer scale variations that deviate from the overall glacial/ interglacial pattern. The total abundance of the *G. truncatulinoides* displays a high value (~500 counts) during glacial interval MIS 6 at ~140 ka. Within interglacial MIS 5, the total counts decrease at MIS 5d (~105 ka) and MIS 5 b (~85 ka). The cold substages decrease and are similar to the modern ocean data but are still higher than during glacial intervals. Additionally, during glacial MIS 4 total counts increases at ~50ka.

4.2 Percent Sinistral

The percent sinistral at Site U1313 generally follows the total abundance trend with high percentages when abundances are high and vice versa (Figure 7c and 7d, respectively). The percent sinistral reaches above 50% when total abundance reaches a maximum, or the percent sinistral drops below 50% when total abundance reaches a minimum. During glacial MIS 6 percent sinistral stays low and does not rise until approximately 135 ka during MIS5. At MIS 3, a percent sinistral maximum occurs even greater than the modern ocean (~40 ka). In contrast, for most of the glacial interval MIS 2, total abundance stays low, and percent sinistral reaches a minimum (0%). The percent sinistral increases during the deglaciation from the last glacial maximum at ~12 ka. The percent sinistral in the modern interglacial period rests slightly above 50%. Overall, each of these trends follows the glacial to interglacial pattern similar to the total abundance.

However, at the finer scale, the percent sinistral results at Site U1313 do not strictly follow the total abundance trend as there are notable differences during MIS 5 and MIS 4 (Figure 7c). During these MIS several intervals present low percent sinistral (<50%), but high total abundance, or vice versa. These major exceptions occur during the interglacial MIS 5 and can be related to its substages. The dextral form becomes the dominant coiling direction at warm intervals MIS 5a (~95 ka) and MIS 5c (~115 ka). The other warm substage, MIS 5e (~120 ka), shows a percent sinistral trend close to 50%, comparable to the percent sinistral during the Holocene. In contrast, the colder substages of MIS 5 (b and d) present high percent sinistral as total abundance decreases but are still >500 which is similar to the total abundance during the Holocene. During the transition from MIS 5 to the glacial period MIS 4 (~70 ka) percent sinistral remains high while total counts are at a minimum. Therefore,

the percent sinistral results at Site U1313 do not strictly follow the glacial/interglacial pattern.

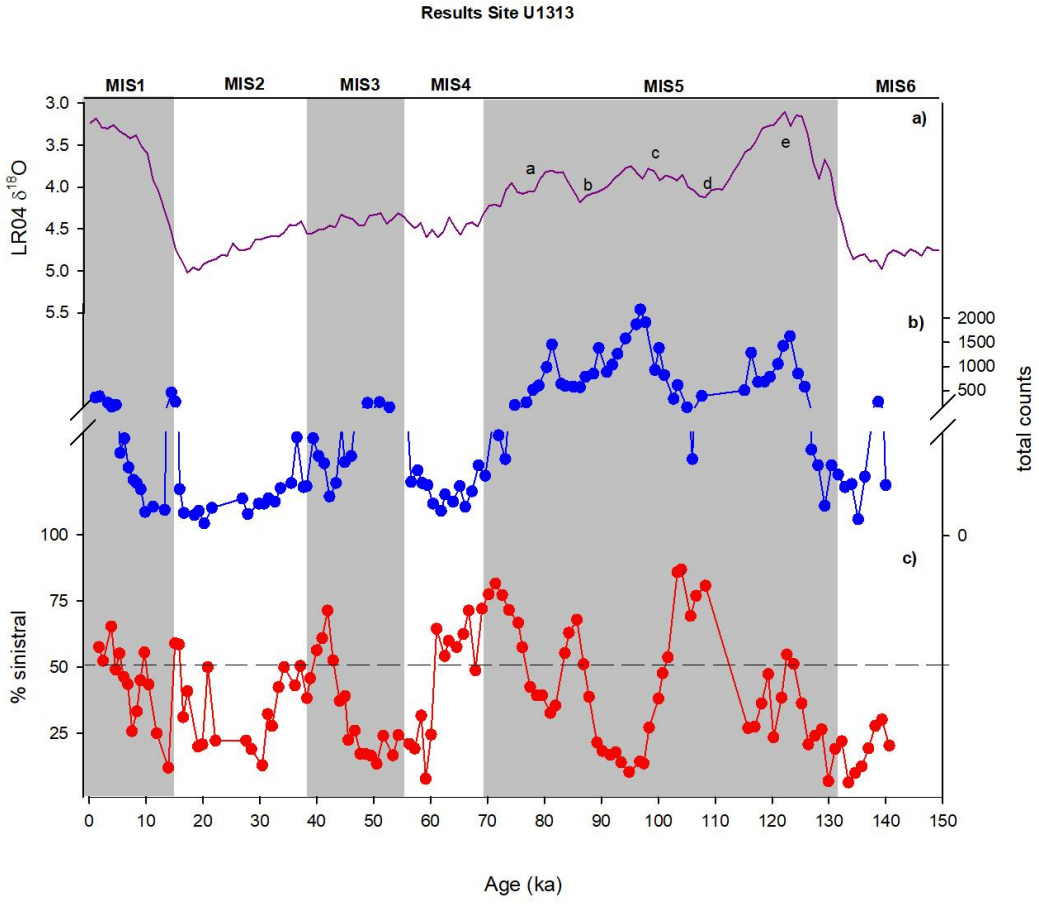

Figure 7: Figure shows total abundance and percent sinistral results at Site U1313. Panels are as follows: a) LR04 benthic age stack spanning 140 ka b) total test count abundance counts of the *G. truncatulinoides*. b) total abundance of *G. truncatulinoides* at site U1313 percent sinistral data of the *G. truncatulinoides*. The horizontal dashed line in c) indicates % sinistral above 50 %. Grey boxes indicate interglacial intervals MIS# and a-e in panel refer to the MIS substage lettering from Railsback et al. (2015)

Chapter 5

DISCUSSION

Over the past 140 ka, the changes in the North Atlantic circulation are due to the glacial/interglacial cycle, as three interglacial intervals and two major glaciations occurred. The interglacial MIS 5 can be compared to our modern interglacial. The major glaciations occurred at 20 ka and 130 ka (MIS 2 and MIS 6), characterized by increased Northern Hemisphere glaciation (Ruddiman, 2014). The circulation of the North Atlantic subtropical gyre during interglacial was previously reconstructed by Billups et al. (2016) and Billups et al. (2020) and was characterized by gyre intensification along the Gulf Stream. In contrast, during the glacial intervals, the northern gyre boundary moved southward towards the equator. Such changes were also reflected in previous studies using different palaeoceanographic proxies that illustrate, glacial cycles, sea surface temperature, and major melting events called Heinrich events (Lisiecki and Raymo, 2005; Stein et al., 2009: Smith et al., 2013; Lang et al., 2016).

5.1 Site Comparison

To see how changes at the northern gyre boundary previously reconstructed compare to changes at the Gulf Stream and the center of the gyre on glacial to interglacial time scales (e.g., Figure 8a), I compared the Site U1313 percent sinistral data to previously published sites KNR140-37 PC and IODP Site 1063 (Figure 8b, c, and d, respectively, and Figure 1 for locations). As mentioned in section 4.3, the percent sinistral results from U1313 show high percent sinistral (>50%) during interglacial intervals and low percent sinistral during glacial intervals, with notable exceptions in MIS 5 and MIS 4 (e.g., Figure 8b). During interglacial MIS 5 percent

sinistral results are variable, with high percent sinistral during the colder intervals of MIS 5 and low percent sinistral (<50%) during the warm intervals. Percent sinistral is close to 50% at MIS 5e, which compares closely to the percent sinistral during the Holocene.

Previously published NOAA Piston Core Site KNR (Billups et al., 2016) (e.g., Figure 1), located beneath the North Atlantic western boundary current, the Gulf Stream, shows percent sinistral results with high percent sinistral in interglacial intervals and low percent sinistral in glacial intervals. Interglacial MIS 5 shows consistently high percent sinistral throughout each substage (Figure 8c), differentiating it from the Site U1313 trend. Similar to Site U1313, the percent sinistral is high in interglacial period MIS 3 and the current interglacial MIS 1 and low in the glacial intervals MIS 4 and 2. Overall, unlike Site U1313 at the northern gyre boundary, this site shows consistent glacial and interglacial patterns for the coiling directions illustrating that the gyre boundary during glacial intervals moves southward toward the equator and remains in a northern position throughout the interglacial intervals.

IODP Site 1063, located in the center of the gyre, shows high percent sinistral in interglacial intervals and low percent sinistral in glacial intervals. Site 1063 is located south of the northern gyre boundary above the Bermuda Rise where sinistral forms dominate in the modern ocean because of the deep permanent thermocline in the central part of the gyre.

The percent sinistral data from Site 1063 follows the trend with high percent sinistral in the interglacial periods and low in the glacial periods (Figure 8b). Like the other two sites percent sinistral results are low (<50%) during the glacial intervals at MIS 2 and MIS 4. The data from Site 1063 during MIS 5 follows closely with the

results from the western boundary current Site KNR140-37 PC but does not follow the percent sinistral results during MIS 5 at site U1313 (Figure 8d). This comparison illustrates that during the last interglacial period (MIS 5) variations in % sinistral at the northern gyre boundary are different from those “upstream” in the western boundary current and the gyre center, which means that the paleoenvironment at the northern gyre boundary at Site U1313 is not directly linked to processes at the lower latitudes such as intensified gyre circulation.

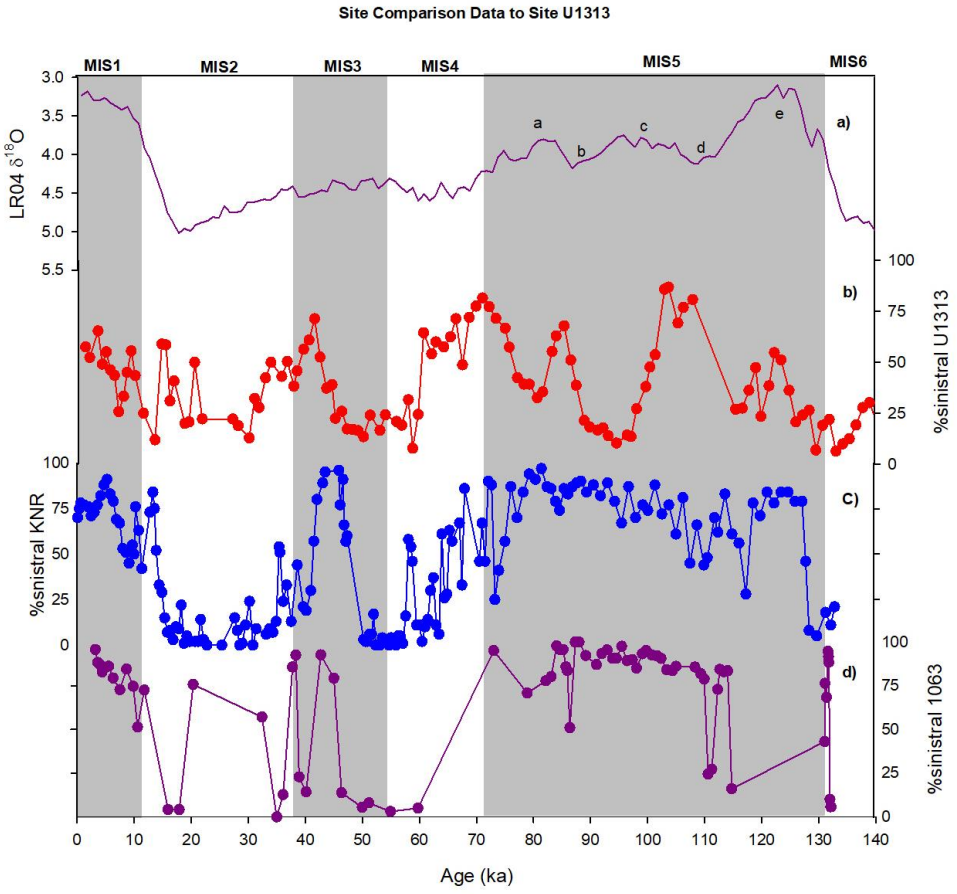

Figure 8: Site comparison data with percent sinistral results from two previously studied sites KNR140-37 PC and IODP Site 1063 (Billups et al. 2016; Billups et al. 2020). Panels are as follows: a) percent sinistral results from our study Site U1313 b) results from KNR140-37 PC; c) results from Site 1063

5.2 Preliminary Interpretation of Gyre Circulation

The difference in percent sinistral during the substages of MIS 5 at Site U1313 compared to the two previously published sites indicates a change in North Atlantic

circulation that affects the warm water advection to Site U1313. Percent sinistral minima occur during the warm stages of MIS 5 with percent sinistral maxima in the cold substages. I speculate that changes in percent sinistral during interglacial period MIS 5 may have to do with the intensification of the gyre or the placement of the North Atlantic Current. Although, I cannot confirm an interpretation until looking at other sites north of Site U1313 that have more direct influence from the North Atlantic Current.

Presences of high dextral forms during interglacial intervals at sites underneath the western boundary current, the Gulf Stream, are observed by Billups et al., (2020) during an older interglacial, MIS 11 (~425 ka to 375 ka). When high dextral counts occur, there are environmental changes characterized by a shallower permanent thermocline. Billups et al. (2020) speculated that the changes were either due to the Gulf Stream located more southeast or an overall intensified flow of the Gulf Stream. Both scenarios cause a shift in the advection of warm water from the Gulf Stream away from the coast leaving the dextral form to dominant at these sites. Our study site, Site U1313, is located on the northern boundary of the North Atlantic Gyre. Since it has surface water influence from the Azores Current and the North Atlantic Current the change in dextral could be from changes in latitudinal placement of the North Atlantic Current or overall intensification changes of the whole gyre. There is no modern analog for the high dextral counts in MIS 5, so it is hard to speculate about specific changes without more study sites from different regions of the gyre or north of the gyre.

Overall, I cannot conclude much information about gyre circulation during MIS 2 and MIS 6 from this proxy at Site U1313. Glacial intervals, and especially the

last glacial interval, had ice sheets reaching much further south in the North Atlantic than during our current interglacial. At previously studied sites western boundary current intensification and southward placement of the gyre were observed (Billups et al. 2016; Billups et al. 2020). Our test abundance counts at site U1313 in glacial intervals MIS 2 and MIS 6 are low. During the glacial periods the dextral form mostly dominates, but there are two instances of higher percent sinistral at 40 ka and 70 ka during MIS 3 and MIS 4. The brief dominance of sinistral forms during the glacial intervals could be due to the intensification or placement of the upper boundaries of the gyre, but because the test abundance counts tend to be lower at these times, we cannot be certain that the variations reflect ideal conditions under which the species flourishes.

5.3 Paleoclimate context at Site U1313

. The two $\delta^{18}O$ records, the LR04 benthic age stack (Figure 9a) and individually published planktic foraminifera $\delta^{18}O$ from *Globigerina bulloides* (Figure 9b), (Smith et al., 2013) illustrate the glacial versus interglacial changes at Site U1313. The LR04 benthic $\delta^{18}O$ age stack provides context to the glacial and interglacial cycles as explained above. The individually published $\delta^{18}O$ from planktic foraminifera G. *bulloides* at site U1313 provide information about surface ocean conditions because G. *bulloides* live in the top mixed layer. In addition to glacial to interglacial ice volume changes, the planktic foraminifera $\delta^{18}O$ values record changes in surface temperature at Site U1313 because a change in 4.2°C can reflect as much as a $\delta^{18}O$ change in 1 $^{0}/_{00}$ (Faure, 1991). The $\delta^{18}O$ values of the G. *bulloides* are generally lower because they are a planktic species and represent the warmer temperatures in the surface water. Overall, the G. *bulloides* record follows the same glacial and

interglacial trend as the LR04 age stack consistent with smaller ice sheets and warmer temperatures during interglacial versus larger ice sheets and colder temperatures during glacial periods. The $\delta^{18}O$ G. *bulloides* record shows the cold and warm substages of MIS 5, with a large contrasting change in $\delta^{18}O$ in MIS 5. The surface temperature change throughout the interglacial MIS5 provides context to the variable hydrography of Site U1313 during this interglacial.

Previously reconstructed sea surface temperatures (SST) at Site U1313 by Stein (2009) span this study's time interval (Figure 9c). The SST trend was determined from alkenone concentration measurements. The low-resolution record of MIS 1-5 was published in supplement to (Stein et al., 2009). The SST at Site U1313 follows a low temperature trend in glacial intervals and a high temperature trend during interglacial intervals. The SST record shows the minimum temperature occurring at the Last Glacial Maximum and the maximum temperatures during MIS 5. This follows closely the $\delta^{18}O$ data from Site U1313 from the global benthic age stack (Figure 9a). Although, due to the lack of data points during MIS 5, there is not enough information to reflect the temperature fluctuations during MIS 5 and its substages that are present in the $\delta^{18}O$ percent sinistral record at Site U1313. A few notable trends occur in the SST data and compare to our percent sinistral results at Site U1313 that follow the glacial and interglacial trend. A distinct cooling trend occurs during MIS4 (~70 ka) after the glacial transition. There is also distinct warming at ~ 5 ka during the current interglacial MIS1.

Ice rafted debris (IRD) data at Site U1313 provides a record of major melting events, or Heinrich ice rafting events, where large terrigenous materials that were once trapped in glacial ice are deposited in sediments. The Heinrich events can be

associated with as much as 4-6 degrees warming (Heinrich, 1988). The published IRD data at Site U1313 from Lang et al. (2016) shows two instances during our study's time interval with IRD maxima (Figure 9d). Ice-rafted debris indicates periods of warming with ice melting occurring after glacial events. The SST trend shows high temperature entering interglacial MIS 5e, which follows the maximum in the IRD record at the end of glacial MIS 6. Temperature maxima occur during MIS 5e (~130 ka) and during MIS 3 (~55 ka). This coincides with two periods of low percent sinistral, with the dextral form dominating at Site U1313. After the first presence of IRD at the beginning of the MIS 6 to MIS 5e transition (~130ka), throughout the rest of MIS 5, percent sinistral is variable (Figure 9e), but the IRD record stays low. The record only shows the two major melting events because site U1313 is at the southernmost reaches of the IRD belt (Lang et al., 2016).

In sum, the percent sinistral at Site U1313 and G. *bulloides* $\delta^{18}O$ record vary together throughout the substages of MIS 5 indicating a coherent change in environmental parameters. The benthic foraminifera LR04 record represents the global ice volume effect on $\delta^{18}O$ and the planktic record represents the change in ice volume as well as surface water temperature effect on $\delta^{18}O$. Therefore, by comparing and subtracting the amplitude of the variations of the $\delta^{18}O$ records I can estimate the sea surface temperature variability because the additional $\delta^{18}O$ change in per mil from substage to substage on the G. *bulloides* $\delta^{18}O$ record represents the surface temperature. Since the difference in the G. *bulloides* $\delta^{18}O$ record amplitude and the benthic $\delta^{18}O$ record is ~ 0.5 $^{0}/_{00}$, and the general relationship between $\delta^{18}O$ and temperature of 1 per mil equals ~4 °C, I can make an estimation that during the MIS 5 substages the surface temperature varies ~2 °C, which is lower than the seasonal

difference in surface temperature change (~6 °C) during the modern ocean (e.g., Figure 2). Because the percent sinistral is high when $\delta^{18}O$ - inferred temperatures are low and the percent sinistral is low when the temperatures are high, this pattern indicates that the thermocline is deeper when the surface waters are cooler, and vice versa. Although, the surface temperature differences between the substages is small, the percent sinistral, and thus the subsurface hydrography varies greatly. Therefore, I can infer that the depth of thermocline is not only sensitive to the surface water temperature at Site U1313, but there are other parameters involved. I do not yet have enough information about the overall changes in hydrography at Site U1313 to understand what is influencing the variations in depth of the thermocline during MIS 5.

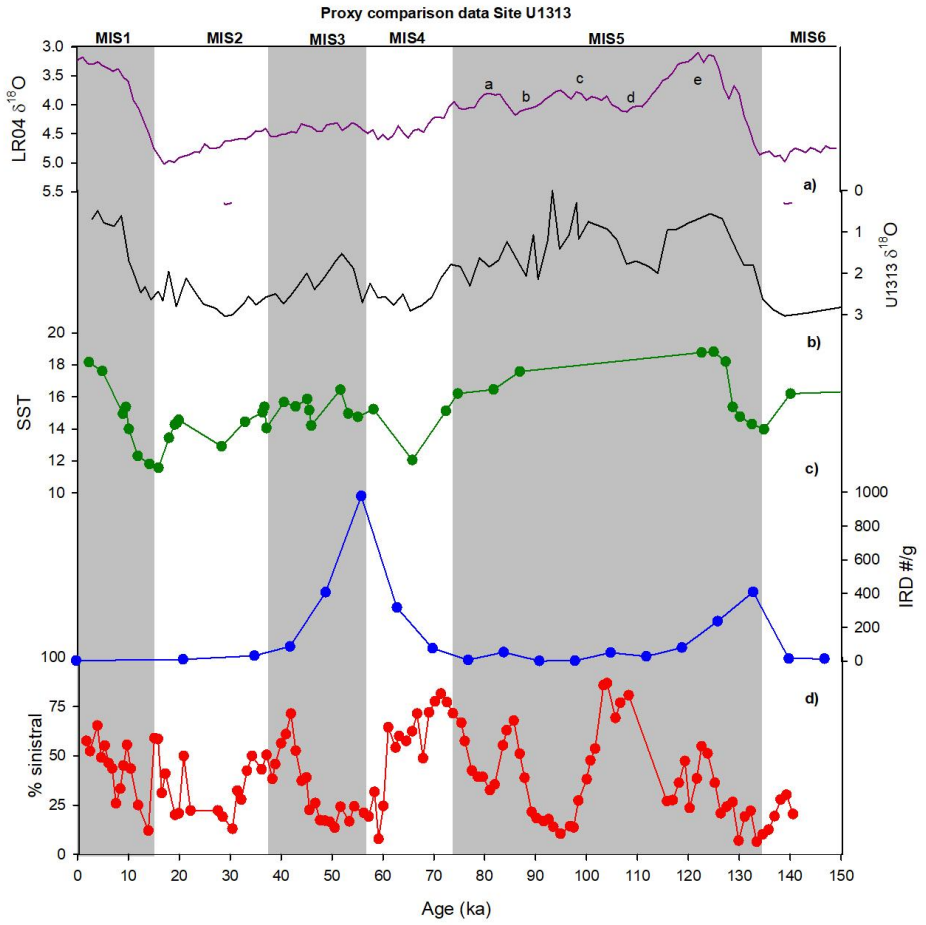

Figure 9: Proxy comparison data with Site U1313. Panels are as follows: a) Lisiecki and Raymo benthic foraminifera age stack (LR04) of $\delta^{18}O$ values (Lisiecki and Raymo, 2005) b) $\delta^{18}O$ values from site U1313 from planktic foraminifera G. *bulloides* (Smith et al., 2013). c) individually published mean based alkenone sea surface temperature (SST) at U1313 (Stein et al., 2009); c) individually published ice rafted debris (IRD) data from Site U1313 (Lang et al, 2016); d) percent sinistral results from site U1313 in this study.

Chapter 6

SUMMARY AND CONCLUSION

My hypothesis stated that relative differences in the coiling ratios of G. *truncatulinoides* over glacial and interglacial intervals would illustrate changes in warm water advection influencing the upper boundary of the gyre over time. To test this hypothesis, I counted the coiling directions of the G. *truncatulinoides* in sediment samples from IODP Site U1313 spanning the past 140 ka. In contrast to published records from lower latitudes, the results from U1313 show that the percent sinistral trend does not strictly follow the interglacial to glacial pattern with notable exceptions during MIS 5. The notable exceptions in the percent sinistral trend occur during the substage of interglacial interval MIS 5 (MIS 5a and 5c), where the dextral form is dominant as the percent sinistral is <50 %. The percent sinistral results at Site U1313 are different than at the previously published sites underneath the western boundary current (Site KNR140-37 PC) and in the center of the gyre (Site 1063). We speculate that the difference in percent sinistral may be due to changes in the longitudinal placement of the North Atlantic Current during MIS 5 or overall intensification of the gyre, but an interpretation cannot be confirmed without additional research using G. *truncatulinoides* as a proxy to understand the role of the North Atlantic Current in the North Atlantic subtropical gyre over glacial cycles. For example, further comparison to more sites in the North Atlantic in the path of the North Atlantic Current and a continuation of the record at Site U1313 needs to occur to better understand hydrographic changes and their relationship to glacial/interglacial climate. Analyzing percent sinistral results at sites north of Site U1313 will provide more context to the lateral movement of the North Atlantic Current.

REFERENCES

Billups, K., Hudson, C., Kunz, H., & Rew., I (2016). Exploring *Globorotalia truncatulinoides* coiling ratios as a proxy for subtropical gyre dynamics in the northwestern Atlantic Ocean during late Pleistocene Ice Ages, *Paleoceanography*, 31, https://doi.org/10.1002/ 2016PA002927.

Billups, K., Vizcaíno, M., Chiarello, J., & Kaiser, E. A. (2020). Reconstructing western boundary current stability in the North Atlantic Ocean for the past 700 kyr from *Globorotalia truncatulinoides* coiling ratios. *Paleoceanography and Paleoclimatology*, 35, e2020PA003958,https://doi.org/10.1029/2020PA003958

Berger, A. (1978). Long-Term Variations of Daily Insolation and Quaternary Climatic Changes, 35(12), 2362-2367, https://doi.org/10.1175/1520-0469(1978)035<2362:LTVODI>2.0.CO;2

De Vargas, C., Renaud, S., Hillbrecht, H., & Pawlowski, J. (2001). Pleistocene adaptive radiation in Globorotalia truncatulinoides: Genetic, morphologic, and environmental evidence. *Paleobiology*, 27(1), 104–125, https://doi.org/10.1666/0094-8373(2001)027<0104:PARIGT>2.0.CO;2

Channell, J.E.T., Kanamatsu, T., Sato, T., Stein, R., Alvarez Zarikian, C.A., Malone, M.J., & the Expedition 303/306 Scientists (2006). *Proceedings of the Integrated Ocean Drilling Program.* Volume 303/306

Emiliani, C. (1955). Pleistocene Temperatures. *The Journal of Geology*, 63(6), https://doi.org/10.1086/626295

Ericson, D., Wollin G., &Wollin, J. (1954). Coiling direction of *Globorotalia truncatulinoides* in deep-sea cores. *Deep Sea Research, 2*, 152-158, https://doi.org/10.1016/0146-6313(55)90018-6

Faure, G. (1991). Principles and applications of inorganic geochemistry :a comprehensive textbook for geology students. *Macmillan Pub. Co.*

Feldmeijer, W., Metcalfe, B., Brummer G., & Gannsen, G. (2014). Reconstructing the depth of the Permanent thermocline through the morphology and geochemistry of the deep dwelling plantonic foraminifer *Globorotalia truncatulinoides. Paleoceanography*, 30, 1-22, https://doi.org/10.1002/2014PA002687

Heinrich, H. (1988). Origin and consequences of cyclic ice rafting in the northeast Atlantic Ocean during the past 130,000 years. Quaternary Res. 29 (2): 142–152. Bibcode:1988QuRes..29..142H, https://doi.org/10.1016/0033-5894(88)90057-9.

Howell, P. (2006). ARAND Time series and spectral analysis package for the Macintosh. Brown Univ.

Kaiser, E. A., Caldwell, A., & Billups, K. (2019). North Atlantic upper-ocean hydrography during the mid-Pleistocene transition evidenced by *Globorotalia truncatulinoides* coiling ratios. *Paleoceanography and Paleoclimatology,* 34. https://doi.org/ 10.1029/2018PA003502

Kucera, M., Rosell-Melé, A., Schneider, R., Waelbroeck, C., & Weinelt, M. (2005). Multiproxy approach for the reconstruction of the glacial ocean surface (MARGO). *Quaternary Science Reviews,* 24(7-9), 813–819. https://doi.org/10.1016/j.quascirev.2004.07.017

Lang, D., Bailey, I., Wilson, P. *et al.* Incursions of southern-sourced water into the deep North Atlantic during late Pliocene glacial intensification. *Nature Geoscience* 9, 375–379 (2016), https://doi.org/10.1038/ngeo2688

Libes, S. M. (2009). An Introduction to Marine Biogeochemistry, Second Edition. *Academic Press.*

Lisiecki, L. E., and M. E. Raymo (2005), A Pliocene-Pleistocene stack of 57 globally distributed benthic $d^{18}O$ records, *Paleoceanograph*y, 20, PA1003, https://doi.org/10.1029/2004PA001071

Marshall, J., Kushner, Y., Battisti, D., Chang, P., Czaja, A., Dickson, R., Hurrell, J., McCartney, M., Saravanan, R., & Visbeck, M, *International Journal of Climatology,* 21(15), https://doi.org/10.1002/joc.693

Milankovitch, M. (1941) Canon Insolation and the Ice-Age Problem. Royal Serbian Academy, *Section of Mathematical and Natural Sciences,* 33, Belgrade.

Quillevere, F., Morard, R., Escarguel, G., Doudy, C., Ujiie, Y., de Garidel-Thoron T., & de Vargas, D. (2011). Glocal same-specimen morpho-genetic analysis of *Truncorotalia truncatulinoides:* A perspective on the morphological species concept in planktonic foraminifera. *Palaeogeography, Palaeoclimatology, Palaeoecology,* 391, 2-12, https://doi.org/10.1016/j.palaeo.2011.03.013

Railsback, L. B., Gibbard, P. L., Head, M. J., Voarintsoa, N. G., Toucanne, S. (2015). An optimized scheme of lettered marine isotope substages for the last 1.0 million years, and the climatostratigraphic nature of isotope stages and substages, *Quaternary Science Reviews,* 111, 94-106, https://doi.org/10.1016/j.quascirev.2015.01.012.

Rahmstorf, S. (2002). Ocean circulation and climate during the past 120,000 years. *Nature* 419, 207–214, https://doi.org/1038/nature01090

Renaud, S., Schmidt, D. N. (2003). Habitat tracking as a response of the planktic foraminifer Globorotalia truncatulinoides to environmental fluctuations during the last 140 kyr, *Marine Micropaleontology*, 49(1–2), 97-122, https://doi.org/10.1016/S0377-8398(03)00031-8.

Ruddiman, W. F., McIntyre, A., & Raymo, M. (1987). Paleoenvironmental results from North Atlantic sites 607 and 609. *Initial Reports of the Deep Sea Drilling Project*, 94. https://doi.org/10.2973/dsdp.proc.94.122.1987

Ruddiman, W. F. (2014) Earth's Climate: Past and Future, Third Edition. *W.H. Freeman and Company: New York.*

Schmitz, W. J., and M. S. McCarthy (1993), On the North Atlantic circulation, J. Geophys. Res., 31, 29–49.

Shackleton, N.J., (1968). Depth of pelagic foraminifera and isotopic changes in Pleistocene oceans. Nature (London) 218, 79–80

Stein, R., Hefter, J. Gru¨tzner, J., Voelker, A. & Naafs B. D. (2009). Variability of surface water characteristics and Heinrich-like events in the Pleistocene midlatitude North Atlantic Ocean: Biomarker and XRD records from IODP Site U1313 (MIS 16–9), *Paleoceanography*, 24, PA2203, https://doi.org/10.1029/2008PA001639

Smith, M. E., Glick, E.V., Lodestro, S. & Rashid H. (2013). Data report: oxygen isotopes and foraminifer abundance record for the last glacial–interglacial cycle and marine isotope Stage 6 at IODP Site U1313, *Proceedings of the Integrated Ocean Drilling Program*, Volume 303/306

Stommel, H. (1948). The Westward Intensification of Wind-Driven Ocean Currents, Transactions, American Geophysical Union, 29(2), https://doi.org/10.1029/TR029i002p00202

Talley., L. D., Pickard G. l. Emery W. J., Swift, J. H. (2011). Descriptive Physical Oceanography, Sixth Edition. *Academic Press.* https://doi.org/10.1016/C2009-0-24322-4

Ujiie, Y., de Garidel-Thoron, T., Wantanabe, S., Wiebe, P., & de Vargas, C. (2010). Coiling dimorphism within a genetic type of planktonic foraminifer *Globorotalia truncatulinoides. Marine Micropaleontology, 77*(3-4), 145-153. https://doi.org/ 10.1016/j.macromicro.2010.09.001

Voelker, A. H. L., Rodrigues, T., Billups, K., Oppo, D., McManus, J., Stein, R., Hefter, J., and Grimalt, J. O. (2010). Variations in mid-latitude North Atlantic surface water properties during the mid-Brunhes (MIS 9–14) and their implications for the thermohaline circulation, *Clim. Past*, 6, 531–552, https://doi.org/10.5194/cp-6-531-2010

Appendix A

DATA TABLE FOR SITE U1313 RESULTS

Sample ID								Meter Composite Depth	Age (ka)	# of splits	# sinistral	# dextral	total counts	% sinistral
303/306	U1313	C	1	H	1	12	14	0.12	1.74	1	102	75	354	57.6
303/306	U1313	C	1	H	1	17	19	0.17	2.47	1	99	90	378	52.4
303/306	U1313	C	1	H	1	27	29	0.27	3.92	0	159	84	243	65.4
303/306	U1313	C	1	H	1	32	34	0.32	4.65	0	79	82	161	49.1
303/306	U1313	C	1	H	1	37	39	0.37	5.37	0	112	91	203	55.2
303/306	U1313	C	1	H	1	42	44	0.42	6.09	0	37	43	80	46.3
303/306	U1313	C	1	H	1	47	49	0.47	6.82	0	41	53	94	43.6
303/306	U1313	C	1	H	1	52	54	0.52	7.55	0	17	49	66	25.8
303/306	U1313	C	1	H	1	58	60	0.58	8.42	0	18	36	54	33.3
303/306	U1313	C	1	H	1	62	64	0.62	9	0	23	28	51	45.1
303/306	U1313	C	1	H	1	67	69	0.67	9.73	0	25	20	45	55.6
303/306	U1313	C	1	H	1	72	74	0.72	10.45	0	6	8	14	42.9
303/306	U1313	C	1	H	1	77	79	0.77	11.18	0	4	7	11	36.4
303/306	U1313	C	1	H	1	82	84	0.82	11.90	0	7	21	28	25.0
303/306	U1313	C	1	H	1	87	89	0.87	12.63	0	2	7	9	22.2
303/306	U1313	C	1	H	1	93	95	0.93	13.57	0	5	6	11	45.5
303/306	U1313	C	1	H	1	96	98	0.96	13.94	0	1	18	19	5.3
303/306	U1313	D	1	H	1	2	4	1.04	15.10	1	135	94	458	59.0
303/306	U1313	D	1	H	1	7	9	1.09	15.82	0	157	111	268	58.6
303/306	U1313	D	1	H	1	12	14	1.14	16.55	0	14	31	45	31.1
303/306	U1313	D	1	H	1	17	19	1.19	17.27	0	9	13	22	40.9
303/306	U1313	D	1	H	1	28	30	1.3	19.15	0	4	16	20	20.0
303/306	U1313	D	1	H	1	32	34	1.34	19.91	0	5	19	24	20.8
303/306	U1313	D	1	H	1	37	39	1.39	20.85	0	5	4	9	55.6
303/306	U1313	D	1	H	1	44	46	1.46	22.21	0	4	8	12	33.3
303/306	U1313	D	1	H	1	47	49	1.49	22.78	0	2	7	9	22.2
303/306	U1313	D	1	H	1	53	55	1.55	23.93	0	2	5	7	28.6
303/306	U1313	D	1	H	1	58	60	1.6	24.89	0	2	5	7	28.6
303/306	U1313	D	1	H	1	62	64	1.64	25.65	0	1	4	5	20.0
303/306	U1313	D	1	H	1	67	69	1.69	26.61	0	2	7	9	22.2

Sample ID									Meter Composite Depth	Age (ka)	# of splits	# sinistral	# dextral	total counts	% sinistral
303/306	U1313	D	1	H	1	72	74		1.74	27.56	0	8	28	36	22.2
303/306	U1313	D	1	H	1	77	79		1.79	28.52	0	4	17	21	19.0
303/306	U1313	D	1	H	1	82	84		1.84	29.48	0	1	7	8	12.5
303/306	U1313	D	1	H	1	87	89		1.89	30.43	0	4	27	31	12.9
303/306	U1313	D	1	H	1	92	94		1.94	31.39	0	10	21	31	32.3
303/306	U1313	D	1	H	1	96	98		1.98	32.16	0	10	26	36	27.8
303/306	U1313	D	1	H	1	102	104		2.04	33.30	0	8	10	18	44.4
303/306	U1313	D	1	H	1	107	109		2.09	34.26	0	23	23	46	50.0
303/306	U1313	D	1	H	1	117	119		2.19	36.17	0	22	29	51	43.1
303/306	U1313	D	1	H	1	122	124		2.24	37.13	0	48	47	95	50.5
303/306	U1313	D	1	H	1	128	130		2.3	38.28	0	18	29	47	38.3
303/306	U1313	D	1	H	1	131	133		2.33	38.85	0	22	26	48	45.8
303/306	U1313	D	1	H	1	137	139		2.39	40	0	53	41	94	56.4
303/306	U1313	D	1	H	1	142	144		2.44	40.96	0	47	30	77	61.0
303/306	U1313	D	1	H	1	147	149		2.49	41.91	0	50	20	70	71.4
303/306	U1313	D	1	H	2	2	4		2.54	42.87	0	20	18	38	52.6
303/306	U1313	D	1	H	2	8	10		2.6	44.02	0	19	32	51	37.3
303/306	U1313	D	1	H	2	13	15		2.65	44.97	0	41	64	105	39.0
303/306	U1313	D	1	H	2	16	18		2.68	45.55	0	16	55	71	22.5
303/306	U1313	D	1	H	2	22	24		2.74	46.70	1	20	57	77	26.0
303/306	U1313	D	1	H	2	27	29		2.79	47.65	0	22	105	127	17.3
303/306	U1313	D	1	H	2	32	34		2.84	48.61	0	24	116	140	17.1
303/306	U1313	D	1	H	2	37	39		2.89	49.57	0	40	202	242	16.5
303/306	U1313	D	1	H	2	42	44		2.94	50.52	0	17	109	126	13.5
303/306	U1313	D	1	H	2	48	50		3	51.67	0	62	195	257	24.1
303/306	U1313	D	1	H	2	57	59		3.09	53.39	0	25	125	150	16.7
303/306	U1313	D	1	H	2	62	64		3.14	54.35	0	25	78	103	24.3
303/306	U1313	D	1	H	2	72	74		3.24	56.26	0	30	113	143	21.0
303/306	U1313	D	1	H	2	77	79		3.29	57.22	0	10	42	52	19.2
303/306	U1313	D	1	H	2	83	85		3.35	58.37	0	20	43	63	31.7
303/306	U1313	D	1	H	2	87	89		3.39	59.13	0	4	47	51	7.8
303/306	U1313	D	1	H	2	92	94		3.44	60.09	0	12	37	49	24.5
303/306	U1313	D	1	H	2	97	99		3.49	61.04	0	20	11	31	64.5
303/306	U1313	D	1	H	2	104	106		3.56	62.47	0	13	11	24	54.2
303/306	U1313	D	1	H	2	107	109		3.59	63.17	0	24	16	40	60.0

Sample ID								Meter Composite Depth	Age (ka)	# of splits	# sinistral	# dextral	total counts	% sinistral
303/306	U1313	D	1	H	2	113	115	3.65	64.58	0	19	14	33	57.6
303/306	U1313	D	1	H	2	118	120	3.7	65.76	0	30	18	48	62.5
303/306	U1313	D	1	H	2	122	124	3.74	66.70	0	20	8	28	71.4
303/306	U1313	D	1	H	2	127	129	3.79	67.87	0	21	22	43	48.8
303/306	U1313	D	1	H	2	132	134	3.84	69.04	0	49	19	68	72.1
303/306	U1313	D	1	H	2	137	139	3.89	70.22	0	45	13	58	77.6
303/306	U1313	D	1	H	2	142	144	3.94	71.39	0	84	19	103	81.6
303/306	U1313	D	1	H	2	147	149	3.99	72.57	0	75	22	97	77.3
303/306	U1313	D	1	H	3	2	4	4.04	73.75	0	53	21	74	71.6
303/306	U1313	D	1	H	3	9	11	4.11	75.39	0	131	65	196	66.8
303/306	U1313	D	1	H	3	12	14	4.14	76.10	0	61	45	106	57.5
303/306	U1313	D	1	H	3	18	20	4.2	77.50	0	108	146	254	42.5
303/306	U1313	D	1	H	3	23	25	4.25	78.68	1	101	156	514	39.3
303/306	U1313	D	1	H	3	27	29	4.29	79.62	1	118	182	600	39.3
303/306	U1313	D	1	H	3	33	35	4.35	81.03	1	160	330	980	32.7
303/306	U1313	D	1	H	3	37	39	4.39	81.97	2	129	234	1452	35.5
303/306	U1313	D	1	H	3	44	46	4.46	83.61	1	176	142	636	55.3
303/306	U1313	D	1	H	3	47	49	4.49	84.32	1	187	110	594	63.0
303/306	U1313	D	1	H	3	53	55	4.55	85.73	1	197	93	580	67.9
303/306	U1313	D	1	H	3	58	60	4.6	86.90	1	145	139	568	51.1
303/306	U1313	D	1	H	3	62	64	4.64	87.84	1	152	240	784	38.8
303/306	U1313	D	1	H	3	68	70	4.7	89.25	1	91	333	848	21.5
303/306	U1313	D	1	H	3	72	74	4.74	90.19	1	126	562	1376	18.3
303/306	U1313	D	1	H	3	78	80	4.8	91.60	2	37	183	880	16.8
303/306	U1313	D	1	H	3	82	84	4.84	92.54	2	46	212	1032	17.8
303/306	U1313	D	1	H	3	86	88	4.88	93.48	2	44	270	1256	14.0
303/306	U1313	D	1	H	3	92	94	4.94	94.89	2	41	353	1576	10.4
303/306	U1313	D	1	H	3	100	102	5.02	96.77	2	67	400	1868	14.3
303/306	U1313	D	1	H	3	103	105	5.05	97.48	3	37	235	2176	13.6
303/306	U1313	D	1	H	3	107	109	5.09	98.42	3	65	174	1912	27.2
303/306	U1313	D	1	H	3	114	116	5.16	100.06	2	88	143	924	38.1
303/306	U1313	D	1	H	3	117	119	5.19	100.77	3	82	90	1376	47.7
303/306	U1313	D	1	H	3	121	123	5.23	101.70	2	110	95	820	53.7
303/306	U1313	D	1	H	3	128	130	5.3	103.35	1	140	23	326	85.9
303/306	U1313	D	1	H	3	131	133	5.33	104.05	2	133	20	612	86.9

Sample ID								Meter Composite Depth	Age (ka)	# of splits	# sinistral	# dextral	total counts	% sinistral
303/306	U1313	D	1	H	3	138	140	5.4	105.70	0	104	46	150	69.3
303/306	U1313	D	1	H	3	142	144	5.44	106.42	0	57	17	74	77.0
303/306	U1313	D	1	H	3	149	150	5.51	108.28	1	156	37	386	80.8
303/306	U1313	A	2	H	1	2	4	5.83	115.80	1	68	184	504	27.0
303/306	U1313	A	2	H	1	7	9	5.88	116.98	2	88	232	1280	27.5
303/306	U1313	A	2	H	1	12	14	5.93	118.15	2	61	107	672	36.3
303/306	U1313	A	2	H	1	17	19	5.98	119.33	2	81	90	684	47.4
303/306	U1313	A	2	H	1	21	23	6.02	120.27	2	46	150	784	23.5
303/306	U1313	A	2	H	1	27	29	6.08	121.67	2	101	161	1048	38.5
303/306	U1313	A	2	H	1	31	33	6.12	122.61	2	195	161	1424	54.8
303/306	U1313	A	2	H	1	36	38	6.17	123.79	3	104	99	1624	51.2
303/306	U1313	A	2	H	1	42	44	6.23	125.20	2	77	135	848	36.3
303/306	U1313	A	2	H	1	47	49	6.28	126.37	2	30	114	576	20.8
303/306	U1313	A	2	H	1	52	54	6.33	127.55	0	20	63	83	24.1
303/306	U1313	A	2	H	1	57	59	6.38	128.72	0	18	50	68	26.5
303/306	U1313	A	2	H	1	62	64	6.43	129.90	0	2	27	29	6.9
303/306	U1313	A	2	H	1	67	69	6.48	131.07	0	13	55	68	19.1
303/306	U1313	A	2	H	1	72	74	6.53	132.24	0	13	46	59	22.0
303/306	U1313	A	2	H	1	77	79	6.58	133.42	0	3	44	47	6.4
303/306	U1313	A	2	H	1	82	84	6.63	134.60	0	5	45	50	10.0
303/306	U1313	A	2	H	1	87	89	6.68	135.77	0	2	14	16	12.5
303/306	U1313	A	2	H	1	92	94	6.73	136.95	0	11	46	57	19.3
303/306	U1313	A	2	H	1	97	99	6.78	138.12	0	30	78	108	27.8
303/306	U1313	A	2	H	1	102	104	6.83	139.29	0	80	185	265	30.2
303/306	U1313	A	2	H	1	107	109	6.88	140.59	0	10	39	49	20.4